HEFAT2014
10th International Conference on Heat Transfer, Fluid Mechanics and Thermodynamics
14 – 16 July 2014
Orlando, Florida

FLOW AND THERMAL CHARACTERISTICS OF AIRFLOW INSIDE A REFRIGERATED CONTAINER

Kayansayan N.*, Alptekin E. and Ezan M.A.
*Author for correspondence
Department of Mechanical Engineering,
Dokuz Eylül University,
Izmir, 35397
Turkey,
E-mail: nuri.kayansayan@deu.edu.tr

ABSTRACT

This study mainly focuses on parametric investigation of ceiling-slot ventilated enclosures for determining the airflow and thermal characteristics. In the analyses, the container cross-sectional area is kept constant. However, the container length assumes values of 6.13 m, 8.33 m, and 13.3 m, and the aspect ratio of the container varies accordingly. Besides, the effect of injection slot width on the flow distribution is also studied by taking two different slot widths at a particular aspect ratio. The air velocity at the slot exit is varied in such a way that the Reynolds number of injection is in the range of 20 and $2x10^5$. The numerical analyses are carried out by using ANSYS-FLUENT software which is based on control volume approach. Reynolds Stress Model is applied for modeling the 3D turbulent flow inside the enclosure. In discretization of convective terms, QUICK scheme is adopted, and SIMPLE algorithm is applied for solution of momentum and continuity equations. For evaluating the turbulent stresses near the wall, "*log-law*" function is used. In heat transfer analysis, for the top, lateral and rear surfaces of the container, the combine effect of solar radiation, convection and surface emission is simultaneously considered. In doing so, 3D flow of air around the truck surface, and the related heat transfer problem is studied by generating thirty-two million of non-uniform grids around the truck. To capture the velocity, pressure and temperature gradients along the boundary layer, special type grids are generated in regions close to the solid surface. Convergence criteria for all flow and temperature parameters are taken to be 10^{-5}. For flows with $Re > 200$, if the container aspect ratio is $H / L < 0.2$, the flow separates from the upper surface of the container at a length ratio of $z / L \approx 0.85$. Otherwise a cone-like vertical vortex occurs and causes uneven flow distribution in the container. The thermal performance of ventilation in the container is measured by a non-dimensional temperature distribution, θ_x at a particular cross-section. Generally, uniformity in temperature is provided at high Reynolds numbers. However, for $H / L < 0.2$, temperature disturbance takes place at the rare surface and can be avoided by full-size injection slot.

NOMENCLATURE

A	[m^2]	Cross-sectional area
c_p	[J/kgK]	Specific heat of air
C's		Turbulence model coefficients
D_H	[m]	Hydraulic diameter of the inlet section, $D_H=4A/P$
E		Energy deviation for evaporator capacity
H	[m]	Height of the container
h	[m]	Vertical size of evaporator
	[W/m^2K]	Convective heat transfer coefficient
I	[%]	Turbulence intensity
k	[W/mK]	Thermal conductivity
	[m^2/s^2]	Kinetic energy of turbulence
L	[m]	Length of the container
l	[m]	Evaporator size
P	[m]	Perimeter
p	[Pa]	Pressure
q	[W]	Heat transferred by a surface or by evaporator
Re		Reynolds number, $Re = \rho V_{inj} D_H / \mu$
S	[W/m^3]	Source term
T	[K]	Local temperature
T_x	[K]	Enthalpy averaged air temperature of a plane at x
W	[m]	Container width
$\overline{u_i u_j}$	[m^2/s^2]	Reynolds stress component
u, v, w	[m/s]	Velocity components
y^+		Non-dimensional wall unit, $y^+ = \frac{y\sqrt{\tau_w/\rho}}{\nu}$
x, y, z	[m]	Cartesian axis directions
Special characters		
α		Surface absorptivity
ε	[m^2/s^3]	Turbulence energy dissipation rate
		Surface emissivity
θ		Non-dimensional local temperature
θ_x		Non-dimensional and enthalpy based temperature of a plane at x

μ	[kgm/s^2]	Dynamic viscosity
ϑ	[m^3/s]	Flow rate
v	[m^2/s]	Kinematic viscosity
ρ	[kg/m^3]	Density of air

Subscripts

in	Evaporator inlet
inj	Evaporator exit
s	Surface
t	Turbulent
i, j, k	Vector directions in *x, y, z*
∞	Surroundings

Superscripts

'	Indicates fluctuations in velocity and temperature

INTRODUCTION

Absence of food refrigeration causes several changes in food structure and accelerates food deterioration. These changes can be in several modes including microbiological type (*growth of microorganisms*), physiological type (*ripening*), biochemical type (*lipid oxidation*), or physical (*loss of moisture content*). An efficient and effective cold-chain is designed for slowing down these changes, and transport refrigeration is one of the vital links in this chain. Because of collecting the refrigeration equipment on one side of the container, and providing relatively easy maintenance, ceiling slot-ventilated type enclosures are usually used in transport refrigeration systems for maintaining the safety and quality of many foods. Air flow patterns provided by such a configuration directly governs the temperature distribution and the heat transfer around the food packages in the refrigerated container.Solid state conductive cooling, being a passive cooling scheme and not being dependent on other support systems, exhibits reliability and volumetric advantages. Even though conductive heat transfer may be orders lower than heat transfer associated with convection or evaporation, its reliability aspect justifies in-depth investigations into cooling methods using this heat transfer mode.

For a constant flow rate of injection, the essential aerodynamic features of air flow inside of a ceiling slot-ventilated and empty enclosure is studied by Moureh et al. [1]. In the analysis, the geometry and the location of cold-air injection device is fixed and located at the top of the front surface. Moreover, the suction slot is at the symmetry line of the front surface but is positioned near to the bottom side. In fact, this type of flow geometry is taken to be invariable throughout their published articles. Similarly, Moureh and Flick [2] performed numerical simulations by using both Reynolds Stress Model (RSM) and the standard *k-ε* model CFD code ANSYS-FLUENT to characterize velocities and air flow patterns within a refrigerated container loaded with two rows of pallets. To avoid the occurrence of stagnant zones in the container, air-duct system is implied and hence enhancement in overall uniformity in temperature distribution throughout the palletised cargo is obtained. In their experiments, a reduced-scale model built with a ratio 1/3.3 of a trailer is used. Good agreement between (RSM) model and the experimental data is found especially at highly turbulent zones. Besides, numerical results accurately predict the point of separation of the blowing wall jet. In their analysis, Tapsoba et al. [3] modelled the food boxes configured inside a ventilated enclosure as slotted boxes. The air flow patterns inside the slotted boxes are studied both numerically and experimentally. As expected, occurrence of high degree of ventilation heterogeneity is determined inside the boxes. However, the presence of slotted walls increases the turbulence level at the rear section of the container. Air flow characteristics above and within the pallets of a loaded container are determined by Moureh et al. [4]. A Laser Doppler Anemometry is used to quantify the pallet ventilation of a container with and without an air duct system.

As shown in Figure 1, this study presents parametric analysis carried out for a ceiling slot-ventilated enclosure with the injection and the suction sections are on the same but at different sides of the cooling device. The cooling device is located at the top of the front surface and is at the symmetry line of the container. In the analysis, the container shape factor (*H*/*L*) varies in the range between 0.19 and 0.38, and the cold air flow Reynolds number is in between 2×10 and 2×10^5. The effect of slot geometry in cooling the container is studied for two different slot-widths which has common acceptance in industrial applications. For half-width injection case, the injection slot is $123\,\text{cm}\times9.6\,\text{cm}$, and the suction slot is $123\,\text{cm}\times23.4\,\text{cm}$, and for full-width injection, the slot dimensions for injection and suction respectively are $246\,\text{cm}\times9.6\,\text{cm}$, and $246\,\text{cm}\times23.4\,\text{cm}$. The purpose of this research is two-fold: the first is to determine the confined flow characteristics of an empty container under the influence of flow Reynolds number as well as the container and the slot geometry. The second deals with evaluating the temperature distribution and the heat gain of air inside the container by describing thermal effects of the flow around a refrigerated truck.

PROBLEM DEFINITION

In determining the flow and heat transfer characteristics of both internal and external airflows of a refrigerated container as depicted in Figure 1, the steady state continuity, time averaged Navier-Stokes and energy equations have to be used as described in the following form,

$$\frac{\partial}{\partial x_i}\left(\rho u_i\right)=0 \tag{1}$$

$$\frac{\partial}{\partial x_j}\left(\rho u_i u_j\right)=-\frac{\partial p}{\partial x_i}+\frac{\partial}{\partial x_j}\left[\mu\left(\frac{\partial u_i}{\partial x_j}+\frac{\partial u_j}{\partial x_i}\right)-\rho\overline{u_i'u_j'}\right] \tag{2}$$

$$\frac{\partial}{\partial x_i}\left(\rho c_p u_i T\right)=\frac{\partial}{\partial x_j}\left[k\frac{\partial T}{\partial x_j}-\rho c_p\overline{u_j'T'}\right]+S \tag{3}$$

where S represents the energy source term and is used in computing the energy generated by the food stored in the container. The air inside the refrigerated space is considered to be an incompressible fluid with constant properties. In modeling the turbulent flow, however, the effective viscosity is defined as the sum of the dynamic viscosity and the eddy viscosity $\left(\rho\overline{u_i'u_j'}\right)$ which represents the effects of turbulent

flow. A similar trend is also applied for the effective thermal conductivity in energy equation.

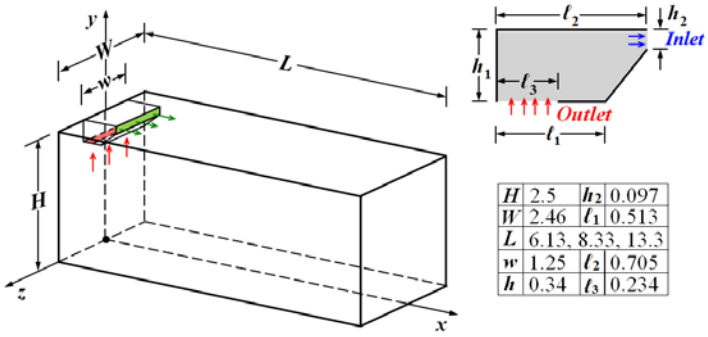

H	2.5	h_2	0.097
W	2.46	ℓ_1	0.513
L	6.13, 8.33, 13.3		
w	1.25	ℓ_2	0.705
h	0.34	ℓ_3	0.234

Figure 1 Definition of the problem

The primary goal of many turbulence models is to find some prescription for the eddy viscosity to predict the Reynolds stresses. Because of solving six equations for the Reynolds stress tensor, and another equation for the dissipation term, the Reynolds Stress Model (RSM) consumes more computational time than the other models. However, RSM is more accurate for flows with separation and reattachment, and provides decent results for air flow patterns inside and outside of the container. There are many versions of RSM, and the one used in the present study is for steady state flow with the absence of buoyancy effects and includes sudden changes in the strain rate, and secondary flows. RSM is expressed in the following form,

$$\frac{\partial}{\partial x_k}\left(\rho u_k \overline{u_i' u_j'}\right) = \left(D_T\right)_{ij} + \phi_{ij} + \varepsilon_{ij} + \frac{\partial}{\partial x_k}\left[\mu \frac{\partial}{\partial x_k}\left(\overline{u_i' u_j'}\right)\right] - \rho\left(\overline{u_i' u_k'}\frac{\partial u_j}{\partial x_k} + \overline{u_j' u_k'}\frac{\partial u_i}{\partial x_k}\right) \quad (4)$$

where $\left(D_T\right)_{ij}$ is the turbulent diffusion term. Lien and Leschziner [5] suggest this term to be in following form,

$$\left(D_T\right)_{ij} = \frac{\partial}{\partial x_k}\left(\frac{\mu_t}{\sigma_k}\frac{\partial \overline{u_i' u_j'}}{\partial x_k}\right) \quad (5)$$

where σ_k assumes the value of 0.82. Similarly the term ϕ_{ij} expresses the pressure strain, and is expressed by Gibson and Launder [6] as following,

$$\phi_{ij} = \underbrace{-C_1\rho\frac{\varepsilon}{k}\left(\overline{u_i' u_j'} - \frac{2}{3}\delta_{ij}k\right)}_{\text{slow pressure strain}} \underbrace{- C_2\left[\left(P_{ij} - C_{ij}\right) - \frac{2}{3}\delta_{ij}\left(0.5P_{kk} - 0.5C_{kk}\right)\right]}_{\text{rapid pressure strain}} + \underbrace{\left(\phi_{ij}\right)_w}_{\text{wall reflection term}} \quad (6)$$

where the wall reflection term is given as,

$$\left(\phi_{ij}\right)_w = C_1'\frac{\varepsilon}{k}\left[\overline{u_k' u_m'} n_k n_m \delta_{ij} - \frac{3}{2}\overline{u_i' u_k'} n_j n_k - \frac{3}{2}\overline{u_j' u_k'} n_i n_k\right]\frac{C_\ell k^{3/2}}{\varepsilon d} + C_2'\left[\phi_{km,2} n_k n_m \delta_{ij} - \frac{3}{2}\phi_{ik,2} n_j n_k - \frac{3}{2}\phi_{jk,2} n_i n_k\right]\frac{C_\ell k^{3/2}}{\varepsilon d} \quad (7)$$

$$C_l = C_\mu^{3/4}/\kappa \quad (8)$$

The constants of pressure strain equation are determined to be $C_1 = 1.8$, $C_2 = 0.6$, $C_1' = 0.5$, $C_2' = 0.3$, $C_\mu = 0.09$ and $\kappa = 0.4187$. The ε_{ij} term in Eq. (4) is the dissipation term and is evaluated as following,

$$\varepsilon_{ij} = \frac{2}{3}\rho\delta_{ij}\varepsilon \quad (9)$$

The parameters, k and ε in Eqs. (7) and (9) need to be modelled by additional equations. More details about the model and the equations to be solved may be found in ANSYS-FLUENT user manual [7].

Boundary Conditions

The flow is uniformly induced into the container at the evaporator exit at a specified temperature and velocity. Throughout the analysis, the temperature of the injected air is kept constant at $T_{inj} = -10°C$. However, to study the entire flow modes, the flow velocity of injection varies in the range between 0.0013 m/s and 13 m/s. Air enters the container as fully developed turbulent flow with 10-percent turbulence intensity at the evaporator exit. Since the flow is fully developed at the inlet and outlet sections, no change in transport properties takes place. Hence, the velocity and temperature gradients $\left(\partial u_i/\partial y, \partial T_i/\partial y\right)$ are assumed to be zero at these regions. In addition, at the symmetry surface of the flow, gradients of all transport properties have to be zero, and no slip condition at the container walls is satisfied by $\left(u = v = w\right)_{wall} = 0$.

Referring to the thermal boundary conditions of the frigorific container, due to extra thickness of the insulation layer at the front and the bottom surfaces, these surfaces are assumed to be adiabatic ($\partial T/\partial n\big|_{wall} = 0$). However, at the top, lateral, and at rear surfaces of the container, the effect of solar radiation and forced convection on heat gain has to be considered. In fact, the energy balance at a particular outer surface may be stated as following,

$$q_{gain} = \alpha I_{solar} - \sigma\varepsilon\left(T_s^4 - T_{sky}^4\right) - h_\infty\left(T_s - T_\infty\right) \quad (10)$$

where T_∞ = 25°C, T_{sky} = -5°C, and $\alpha = \varepsilon = 0.96$ for the metallic substrate. Suppose that the outer surface heat transfer coefficient is pre-determined. Then, for an assumed value of T_s, the surface heat gain may be calculated by Eq. (10). The resulting heat gain is utilized at the interior surface energy balance to calculate a new value for the surface temperature, T_s, which has to be compared with initially assumed value. Hence, trial-and-error method of solution of Eq. (10) determines the surface temperature that is the thermal boundary condition for the interior flow. In evaluating the heat transfer coefficient, h_∞ at the outer surfaces of the container, however, the external flow around the refrigerated truck should be studied.

External flow around a refrigerated truck

As shown in Figure 2, an appropriate solution domain is to be established by considering the approximate size of the

pressure built up region in front of the truck, and the maximum size of vorticities occurring on the top, lateral and rear surfaces of the container. Atmospheric air at temperature, T_∞ = 25°C enters the computational domain uniformly at a particular velocity V_∞, which assumes orderly values of 0.1 m/s, 10 m/s, and 25 m/s in the analysis. At the inlet surface, the flow turbulence intensity, I and the turbulent viscosity ratio, μ_t/μ is assumed to be 2-percent, and 10 respectively. At the exit of the computational domain, however, flow is fully developed and no change in transport properties takes place. Similarly, at the symmetry surface, gradients of all transport properties are at zero value.

As shown by the enlarged view that is indicated by C in Figure 2, to be able to compute high gradients of flow and heat transfer in the vicinity of walls, boundary layer meshes with high mesh densities are used. The meshes around the truck walls and along the ground surface start with a size of 6 mm. The size gradually increases to 10 mm within 20 layers of quadrilateral meshes. The rest of the computational domain is filled with tetrahedral meshes. Hence, the number of grid points used for analyzing the external flow accumulates to 32×10^6 .

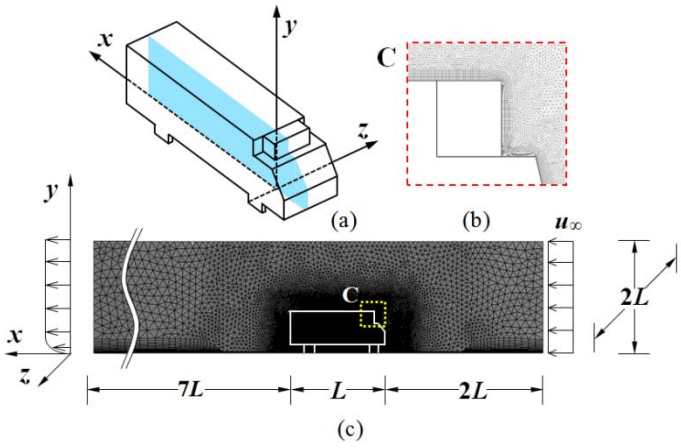

Figure 2 (a) 3D view and the symmetry plane of a typical truck, (b) External flow mesh distribution, (c) details of mesh size

SOLUTION METHOD

The mathematical model is built by using ANSYS-FLUENT, the commercial CFD software which is a finite volume general purpose CFD code. The pressure correction algorithm SIMPLE is used in solving Navier-Stokes equations and the transport equations of turbulent quantities.

In internal flow analysis of the container, computations start with k-ε turbulence modelling applied to governing equations that are discretized by the second order upwind scheme. Convergence is assessed based on the normalized rms value of the residuals of all variables. When this value reaches 10^{-5} for all variables, first, the discretization scheme is changed to QUICK method, and then the turbulence modelling is converted to Reynolds Stress Model (RSM) in the analysis. For the entire analysis, default values of relaxation factors are used in computations.

In modelling the flow external to the frigorific truck, not only the size of the computational domain; length (z = 101.5 m) × height (y = 20.3 m) × depth (x = 20.3 m) but also the number of equations involved in RSM model affect the model to be implemented in decision making stage, and the realizable model has been used. For flows featuring strong vortices, and rotation, the realizable k-ε model shows substantial improvements over the standard k-ε model by addressing a new dissipation function [8]. Similar to internal flow analysis, the second order upwind scheme is adopted in discretization of governing equations, and the log-law function as proposed by Launder and Spalding [9] is used for boundary layer treatment. Due to large number of grid points of the computational domain, the computations have been carried out by Intel Xeon, model no.X5650 high performance computer cluster system (HPC) which provides 48 GB RAM, and is equipped with 24-core, 2.67 GHz processor. At a particular vehicle speed of V_∞, eight cores of (HPC) simultaneously work for a time period of one week to get converged results.

Wall treatment

The automatic wall function given in ANSYS-FLUENT user manual is appropriate for low Reynolds number turbulent models. In fact, this function considers the laminar viscous-sublayer and shifts gradually between the laminar viscous sublayer and the logarithmic wall function [9]. Hence, the model provides an analytical solution for both the linear laminar sublayer and the logarithmic layer. Due to high values of velocity and temperature gradients along the surfaces, densely located quadrilateral meshes with 10-percent growth rate are assumed to be appropriate for the wall treatment. Thus the maximum value of y^+ does not exceed 150 for the considered all mesh sizes.

Validation

The numerical scheme developed for the current study is validated by the experimental work of Moureh and Flick [10] by generating similar data at the same flow conditions and for the same geometry. Moureh [10] carried out his velocity measurements by Laser Doppler Anemometry (LDA) at 1080 points of the container volume having the dimensions of 2.46 m (*width*) × 2.5 m (*height*) × 13.3 m (length). The container experimented by Moureh is numerically simulated by mesh distribution of 100 (*width*) × 106 (*height*) × 250 (*length*) which accumulates to a total of 2.65×10^6 nodal points. In Figure 3, lengthwise variation of air injection velocity at the slot centerline is depicted and compared with the experimental data.

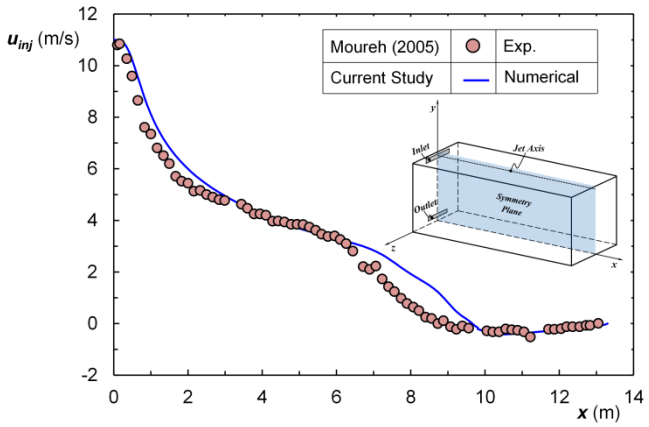

Figure 3 Decay of jet velocity

After exiting the evaporator, the air jet expands. Due to entrainment of the surrounding air, however, the jet centerline velocity decays up to $x \approx 3$ m, and assumes approximately constant values until the point of separation has reached. Such behavior of injected air is also consistent with the lengthwise variation of the maximum jet velocity.

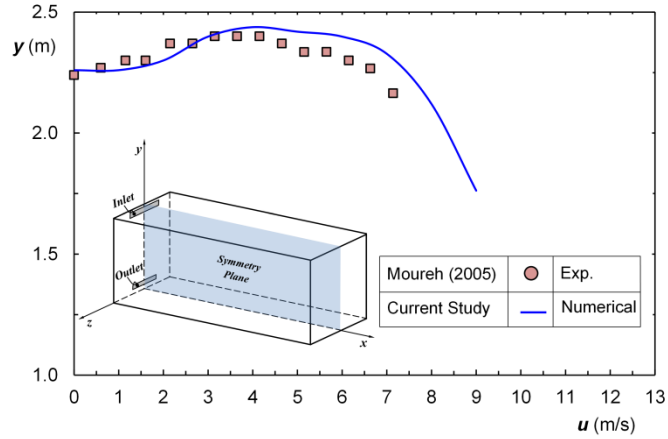

Figure 4 Variation of maximum velocity height along the lengthwise of the container

As shown in Figure 4, due to Coanda effect, the maximum jet velocity moves toward the ceiling as the air jet travels lengthwise, and for $x > 3$ m, its position is kept constant up to the point of separation. In both figures and for the entire range of measurements, the numerical findings are in good harmony with the experimental data. However, in a region close to the point of separation, a discrepancy between the experimental and numerical results is noted. Figure 5 compares the variation of velocity profiles at the symmetry plane of *u*-component at several *x* values respectively. In this figure, the numerical data are also in good agreement with the experimental findings of Moureh [10]. As the flow approaches to the recirculation zone, however, deviation occurs between both set of data, and the numerical results underestimate the velocities in a region close to the point of separation.

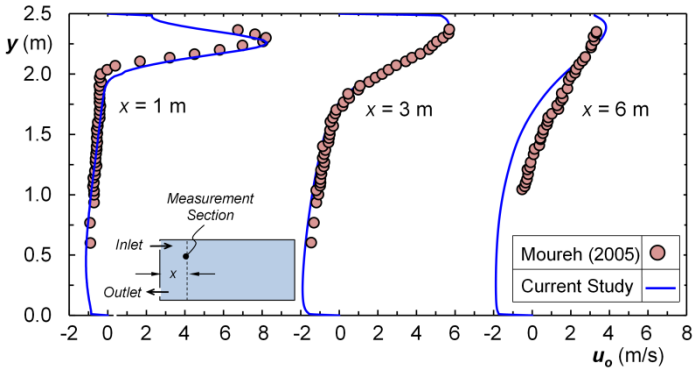

Figure 5 Lengthwise variation of the velocity profiles

Mesh Independency

Mesh independent solutions are sought for all configurations. In order to resolve the high gradients of both velocity and thermal boundary layers in the vicinity of walls and corners, meshes with high mesh densities structured in rectangular shape are used. The container configured as 2.46 m (*width*) x 2.5m (*height*) x 8.33 m (*length*) with the flow geometry as depicted in Figure 1 is used for mesh independence analysis. The number of meshes is refined successively starting at 2.4×10^6 to 4.6×10^6 and 10×10^6. Starting at the evaporator exit, the lengthwise variation of jet centreline velocity is compared with the corresponding finer mesh in each case. As illustrated in Figure 6a, the difference between the velocity values accumulates in an uncertainty band of ±2% width. Similarly, the consistency of the data in Figure 6b for velocity profiles at several locations indicates the mesh independence. When the deviation between the velocity values is found to be less than ±2% then the results are accepted as mesh independent. Based on this criterion, the mesh selected for the current study has a number of grid points about 2.4×10^6.

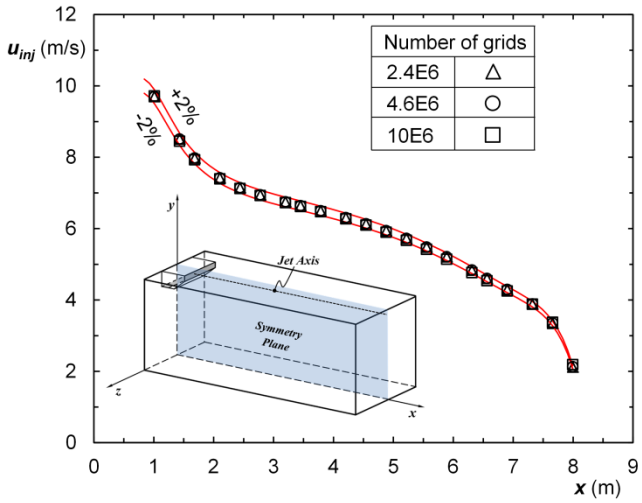

(a) Comparison along the jet axis

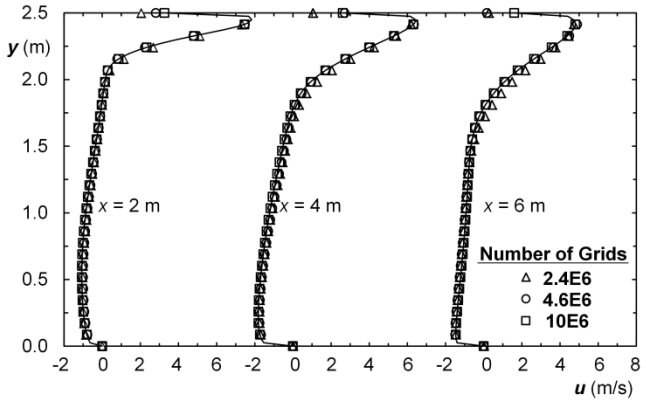

(b) Comparison of velocities at several *x*-locations

Figure 6 Mesh independency

RESULTS AND DISCUSSION

For a particular injection and suction geometry, the flow and heat transfer characteristics of air inside the container depends on the air injection Reynolds number, Re, and the container aspect ratio, *H/L*. In parametric analysis, quadrilateral mesh type is used for the entire container volume. In selecting the grid size, however, limits of law of wall principle are satisfied ($y^+ < 500$). Hence, the mesh distribution of the solution domain is taken to be as, 79 (*width*) x 120 (*height*) x 303 (*length*). The first part of the analysis is about determining the flow characteristics and then the second part deals with heat transfer properties of the flow.

Flow analysis

Figure 7 illustrates the effect of Reynolds number on flow for a container having an aspect ratio of 0.3. At low Reynolds number (Re = 200), the jet flow separates from the ceiling at *x/L* = 0.70, and forms a secondary circulation zone near the rear side of the enclosure. As the Reynolds number increases (Re = 2000), Coanda effect on the jet becomes dominant, the size of secondary circulation zone decreases and the jet separates from the ceiling at *x/L* = 0.85. No separation of flow is noted at higher Reynolds numbers. However, as explained on Figure 7(d), a secondary vortex develops vertically close to the rear surface of the container and becomes more intense at higher Reynolds numbers. This funnel-like vortex certainly disturbs the flow and causes uneven flow distribution in a region close to the rear-side of the container. Since the suction of air is accomplished at the bottom surface of the evaporator, the size of suction zone enlarges as the Reynolds number increases.

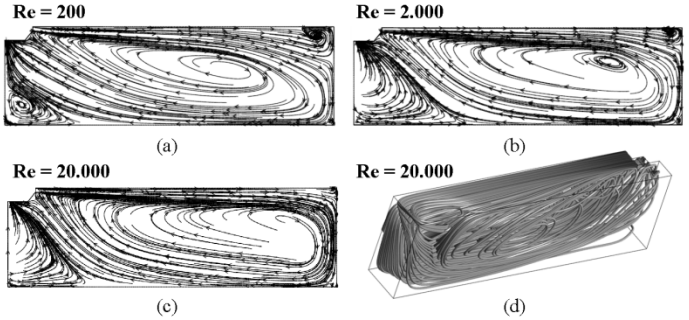

Figure 7 Effect of Re number on the air flow characteristics

To illustrate the effect of Reynolds number on the ventilation efficiency of the container, the longitudinal variation of non-dimensional air flow rate $\vartheta_x / \vartheta_{inj}$ is provided in Figure 8. In this figure, the circulation flow rate, ϑ_x at a particular cross-section along the container is calculated as,

$$\vartheta_x = 0.5 \int_A |U| dA \qquad (11)$$

As can be seen by Figure 8, increase in Reynolds number reduces the confinement effect and increases the ventilation. Moreover, the maximum value of $\vartheta_x / \vartheta_{inj}$ sweeps to the right at higher Reynolds numbers, starting with *x/L* = 0.52 for Re = 200 and ends with *x/L* = 0.70 at Re = 200.000. As stated previously, increase in Reynolds number intensifies the vertical vortex which disturbs the ventilation and resolves with a secondary peak in Figure 8. The effect of container aspect ratio, *H/L* on ventilation is studied in Figure 9 for Re = 20.000. As expected, the container ventilation enhances as the aspect ratio increases, and results with a broader region in the container that satisfies the condition of $\vartheta_x / \vartheta_{inj} > 1$. The behaviour of poor ventilation at aspect ratio of 0.188 has to be alleviated by redesigning the flow system of the container.

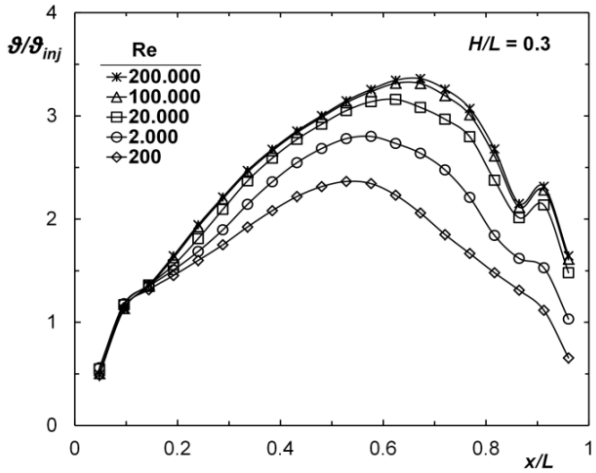

Figure 8 Effect of Re number on the ventilation efficiency

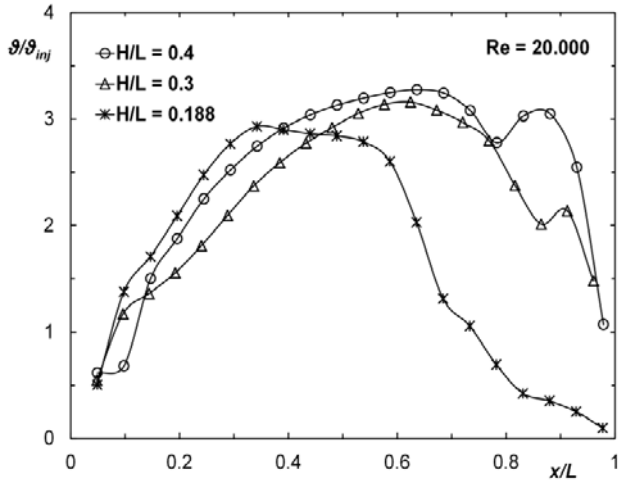

Figure 9 Effect of aspect ratio on the ventilation efficiency

In the analysis, the effect of injection slot size on ventilation is also studied. Figure 10a provides an isometric view of streamlines and compares the flow behaviour for half-size and full-size injections. At the same Reynolds number and aspect ratio, no cone-like vertical vortex occurs at the rear region of the container for full-size injection. Figure 10a shows that airflow is more uniformly distributed at full-size injection relative to that of half-size. In fact, as described clearly by Figure 10b, due to absence of vertical vortex, air ventilation becomes more efficient by full-size injection and no secondary peaks appear in the lengthwise distribution.

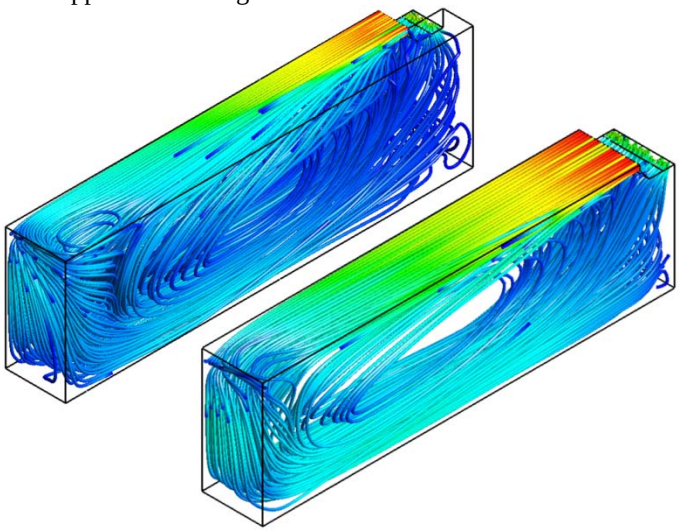

(a)

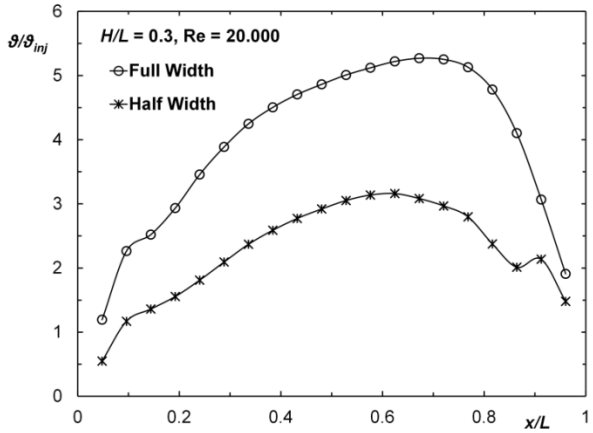

(b)

Figure 10 Effect of injection width on (a) the ventilation efficiency and (b) air flow distribution

Heat transfer analysis

In solving the energy equation for the specified container domain, first the container surfaces are assumed to be at constant temperature and then the temperature distribution of airflow in the container is computed. The surface heat fluxes are calculated accordingly. Since the heat transfer coefficients of outer surfaces are pre-determined by the external flow analysis, Eq. 10 may be resolved for surface temperature at a particular surface heat gain, q_{gain}. Hence, considering the new values of surface temperatures, the temperature distribution in the container is recalculated and the procedure is repeated until the temperature difference within the solution domain becomes less then10^{-3}. Figure 11 presents typical non-dimensional temperature patterns of airflow in the container. All temperatures considered in this figure are at lengthwise symmetry plane of the container, and local value of non-dimensional temperature θ is defined as,

$$\theta = \frac{T_{in} - T}{T_{in} - T_{inj}} \tag{12}$$

Figures 11a and 11b compares the effect of Reynolds number on isotherms, and indicates that isotherms with higher θ-values occupy larger portion of the container volume at higher Reynolds numbers. Moreover, comparison of Figures 11b and 11c reveals the effect of container aspect ratio on the temperature distribution. Because of flow separation at lengthwise direction for $H / L = 0.188$, air becomes stagnant in a region close to the rear side of the container. An undesirable case with temperatures higher than the temperature at the evaporator inlet takes place. Hence, as shown in Fig. 11c, negative θ-values are recorded.

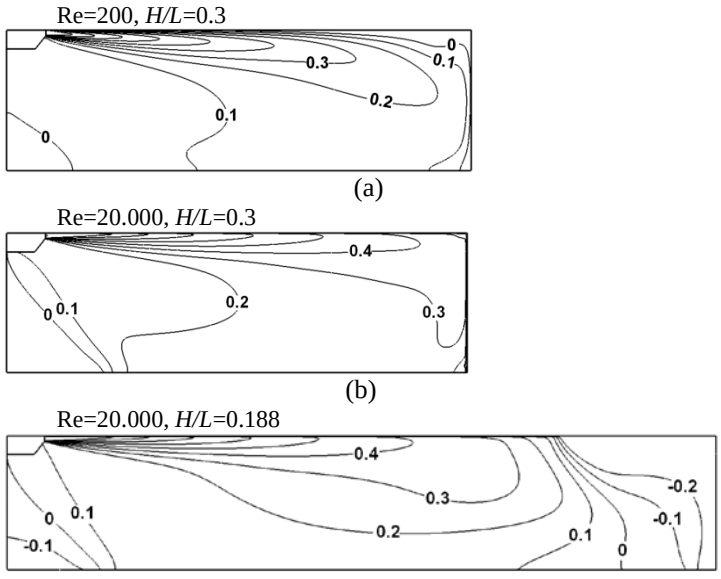

(a) (b) (c)

Figure 11 Effect of Reynolds number and aspect ratio on container temperature distribution

The mass weighted average temperature of airflow in the container is determined as,

$$T_x = \frac{\int_A \rho c_p T |U| dA}{\int_A \rho c_p |U| dA} \tag{12}$$

This temperature represents the enthalpy averaged temperature of a cross-section at x, and can be non-

dimensionalized with respect to maximum temperature difference, $(T_{in} - T_{inj})$ as,

$$\theta_x = \frac{T_{in} - T_x}{T_{in} - T_{inj}} \qquad (13)$$

The effect of Reynolds number on enthalpy averaged temperature is represented in Figure 12.

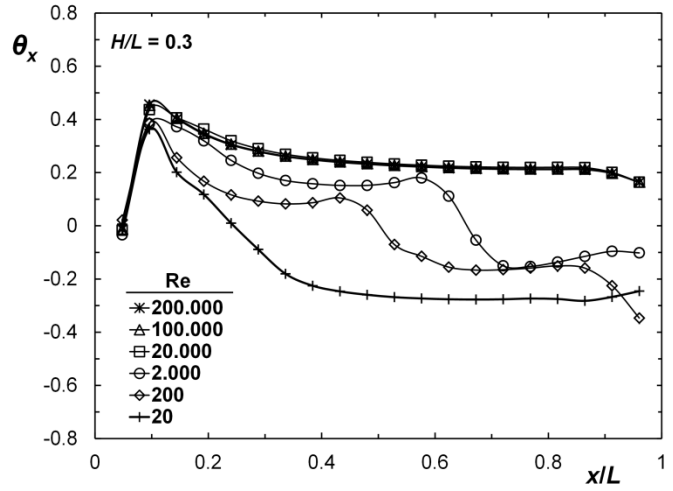

Figure 12 Effect of Re number on enthalpy averaged temperature distribution

Due to increase of ventilation at high Reynolds numbers, the temperature distribution within the container is more uniform and θ_x-values are above zero. In fact, for $Re \geq 20.000$, the effect of Reynolds number on temperature is not distinct as the effect at $\mathrm{Re} \leq 20.000$. The occurrence of vertical vortex disturbs the temperature uniformity and ends with negative θ_x value in a region close to the rear surface $x / L > 0.7$. Negative θ_x-value indicates the existence of hot spot within the container and represents poor performance.

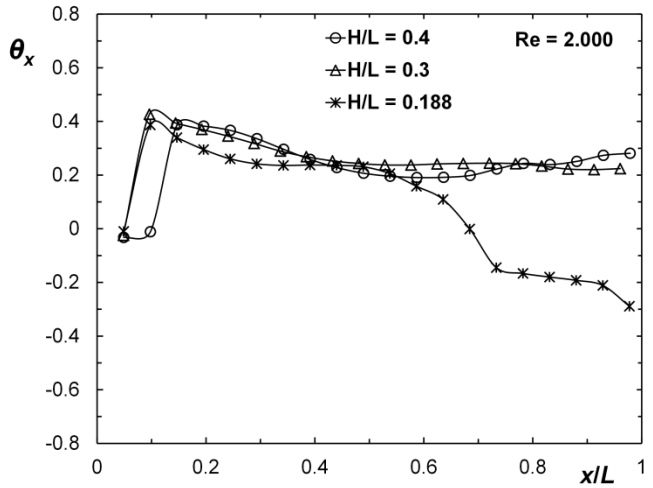

Figure 13 The lengthwise variation of enthalpy averaged temperature at a particular flow rate.

The effect of aspect ratio, *H/L*, on container temperature distribution is shown in Fig. 13. As it may be noticed for $H / L = 0.188$, due to flow separation at *x/L* = 0.60 for Re = 2000, the temperature uniformity is disturbed and undesirable negative θ_x-values are registered for the recirculation zone.

Figure 14 illustrates the effect of injection slot size on temperature distribution of air for a particular Reynolds number and container aspect ratio. In accord with the flow characteristics, full injection avoids development of a region with negative θ_x-values, and uniformity of temperature within the container is maintained.

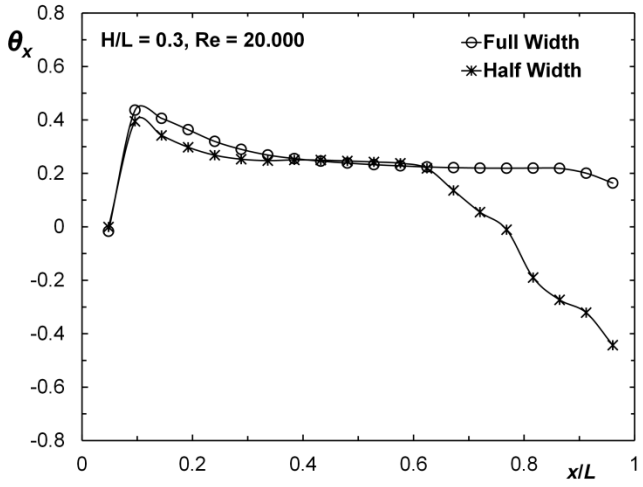

Figure 14 Effect of injection width on temperature uniformity in the container

Figure 15 reflects the effect of changing the injection slot size on evaporator capacity and compares the variation of evaporator capacities with respect to flow Reynolds number for both slot widths at an aspect ratio of 0.3.

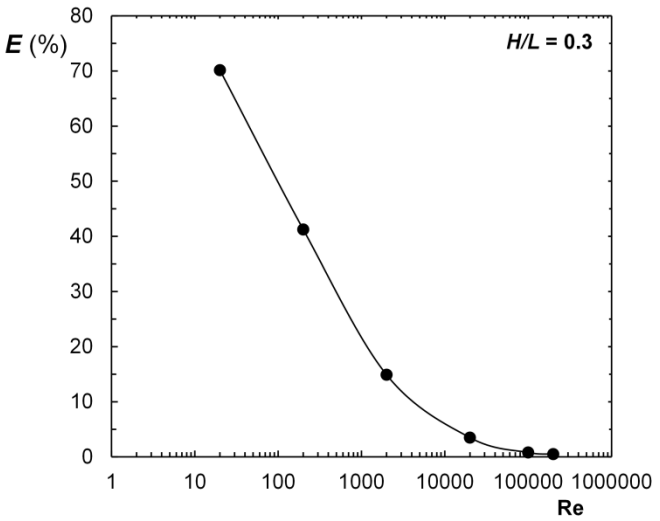

Figure 15 Effect of Reynolds number on evaporator capacity for two different slot-widths

Referring to half and full size evaporator designs, the deviation of energy consumption at the evaporator, *E*, is defined as following,

$$E = \frac{q_{full} - q_{half}}{q_{half}} \times 100\% \quad (14)$$

As can be seen by Fig. 15, the evaporator with full slot width always consumes more heat than half-size evaporator at the same Reynolds number. However, as the Reynolds number increases, the deviation in heat requirement for evaporator decreases, and at the limit, the deviation, *E*, assumes a minimum of 0.5% at Re = 200.000.

CONCLUSION

Within the scope of parameters studied in this article, at high Reynolds numbers of airflow and at high values of container aspect ratios, the flow ventilation becomes better and the heat transfer conditions are enhanced in a refrigerated truck. Analysis reveals that even better enhancement in flow characteristics results with full-size injection system. In industrial applications, the evaporator of a refrigerated truck runs at Reynolds numbers varying in a range between 100.000 and 200.000. Considering this fact, since the full-size injection provides uniform flow and temperature characteristics at all aspect ratios, the performance of full-size injection system is much better for efficient logistics of perishable goods.

Acknowledgement

This research is supported by Republic of Turkey Ministry of Science, Industry and Technology under the grant number: 01114.STZ.2011-2 and Dokuz Eylül University Scientific Research Foundation Grant BAP-Project number: 2013.KB.FEN.9.

REFERENCES

[1] J. Moureh and D. Flick, Wall air-jet Characteristics and air flow patterns within a slot ventilated enclosure, Int. J. Thermal Sciences, Vol.42, 2003, pp. 703-711.

[2] J. Moureh and D. Flick, Airflow patterns and temperature distribution in a typical refrigerated truck configuration loaded with pallets, Int. J. Refrigeration, Vol.27, 2004, pp. 464-474.

[3] M. Tapsoba, J. Moureh, and D. Flick, Airflow Patterns in a Slot-Ventilated Enclosure Partially Loaded with Empty Slotted Boxes, Int. J. Heat and Fluid Flow, Vol.28, 2007, pp. 963-977.

[4] J. Moureh, S. Tapsoba, E. Derens, and D. Flick, Air Velocity Characteristics within Vented Pallets Loaded in a Refrigerated Vehicle with and without Air Ducts, Int. J. Refrigeration, Vol.32, 2009, pp. 220-234.

[5] F.S. Lien and M. A. Leschziner, Assessment of Turbulent Transport Models Including Non-linear RNG Eddy-Viscosity Formulation and Second Moment Closure, Computers and Fluids, Vol.23, no.8, 1994, pp. 983-1004.

[6] M.M. Gibson, and B.E. Launder, Ground Effects on Pressure Fluctuations in the Atmospheric Boundary Layer, J. Fluid Mech., Vol.86, 1978, pp.491-511.

[7] ANSYS-FLUENT 14.0 User Guide, ANSYS Inc., 2009.

[8] T.H. Shih, W.W. Liou, A. Shabbir, Z. Yang, and J. Zhu, A New k-ε Eddy-Viscosity Model for High Reynolds Number Turbulent Flows-Model Development and Validation, Computers and Fluids, Vol.24, no.3, 1995, pp. 227-238.

[9] B.E. Launder, D.B. Spalding, Numerical Computation of Turbulent Flows, Computer Methods in Applied Mechanics and Engineering, Vol. 3, 1974, pp. 269-289.

[10] J. Moureh, and D. Flick, Airflow Characteristics within a Slot-Ventilated Enclosure, Int. J. Heat and Fluid Flow, Vol. 26, 2005, pp. 12-24.